JVST B
Journal of Vacuum Science & Technology B

Optimization of the response time measuring method for liquid crystal variable retarders

Cite as: J. Vac. Sci. Technol. B **37**, 062930 (2019); https://doi.org/10.1116/1.5122786
Submitted: 31 July 2019 . Accepted: 05 November 2019 . Published Online: 03 December 2019

Antonio Campos-Jara, Pilar García Parejo, and Alberto Álvarez-Herrero

Optimization of the response time measuring method for liquid crystal variable retarders

Antonio Campos-Jara,[1] Pilar García Parejo,[2] and Alberto Álvarez-Herrero[1,a)]
[1]*Instituto Nacional de Técnica Aeroespacial, Space Optical Instrumentation Area, Crta. de Ajalvir KM4, Torrejón de Ardoz, Madrid 28850, Spain*
[2]*Ingeniería de Sistemas para la Defensa de España, External Consultant for INTA, Beatriz de Bobadilla 3, Madrid 28040, Spain*

(Received 31 July 2019; accepted 5 November 2019; published 3 December 2019)

Liquid crystal variable retarders (LCVRs) have been extensively used as light polarization modulators for ground-based polarimetric applications. Shortly, LCVRs will be used as polarization state analyzers in two instruments onboard the Solar Orbiter mission of the European Space Agency. Both ground- and space-based polarimeters require LCVR response time values that fulfill the required image acquisition rate of the polarimetric measurements. Therefore, it is necessary to have a reliable method to measure the LCVR optical retardance response times. Response times are usually estimated via optical methods using crossed or parallel polarizers. Nevertheless, these methods measure light intensity transitions to infer the response time instead of directly measuring the changes in the optical retardance. In this work, an experimental setup that uses a Soleil-Babinet variable compensator is proposed. On one hand, this allows one to study the effect of the nonlinear dependence of the light intensity on the optical retardance in the response time determination, which is neglected in most works. On the other hand, the use of the variable compensator allows one to measure the LCVR response times in the highest sensitivity areas of the system that minimizes the uncertainty of the measurement. The six transitions for the Polarimetric and Helioseismic Imager instrument modulation scheme of a representative LCVR have been measured. Based on the results, the optimized conditions to measure response times are found, which can be achieved by using the variable compensator and an IR wavelength ($\lambda = 987.7$ nm) as proposed in the experimental setup.
https://doi.org/10.1116/1.5122786

I. INTRODUCTION

Liquid crystal variable retarders (LCVRs) have been extensively used as light polarization modulators for ground-based polarimetric applications.[1–6] The Solar Orbiter mission of the European Space Agency will be the first space mission that will use LCVRs onboard its payload. In this mission, they will be used as polarization state analyzers (PSAs) in two scientific instruments: PHI[1,2] (the Polarimetric and Helioseismic Imager for Solar Orbiter) and METIS[1,3] (Multi Element Telescope for Imaging and Spectroscopy). Both ground- and space-based polarimeters require the accurate determination of the LCVR response times at the specific LCVR transitions of the instruments' modulation schemes. For the specific case of the Solar Orbiter mission, the LCVR response time shall be lower than 100 ms for all the transitions, taking into account all the environmental conditions of the mission. Therefore, it is necessary to have a reliable method to measure the LCVR optical retardance response times in order to fulfill the required image acquisition rate during the mission. The response time is usually estimated via transmitted light measurement methods using crossed or parallel polarizer setups.[7,8] Nevertheless, these methods measure light intensity as a function of time and show a sinusoidal dependence on the optical retardance changes. This dependence is neglected in most works. Additionally, the sensitivity to determine the response times of the optical retardance extracted from the light intensity measurement is different along the curve and must be taken into account. For this reason, an experimental setup that uses a Soleil-Babinet compensator is proposed in this work. The Soleil-Babinet variable compensator allows tuning the optical retardance starting point of the response time measurements. In this way, we can study the effect of this dependence on the optical retardance response times measured, as well as the sensitivity to determine them. In addition, the experimental setup uses a longer wavelength ($\lambda = 987$ nm) than the PHI operative wavelength ($\lambda = 617.3$ nm). In this way, we reduce the optical retardance change of all the LCVR transitions studied below π radians, avoiding overtaking a maximum in the light intensity sinusoidal signal and then simplifying the transitions measurement analysis.

This study and the experimental setup proposed allow us to properly select the parameters to measure the optical retardance response times maximizing the sensitivity to determine them. Additionally, an accurate determination of the variation of the LCVR optical retardance as a function of time allows us to calculate accurately the temporal variation of the liquid crystal (LC) molecules' mean tilt. It will allow

Note: This paper is part of the Conference Collection: 8th International Conference on Spectroscopic Ellipsometry 2019, ICSE.
a)Electronic mail: alvareza@inta.es

us to investigate the liquid crystal molecular dynamics under the influence of the space environment conditions afterward. In conclusion, a deeper understanding of the method sensitivity and how this affects the response time measurements allow defining experimental setups and optimal conditions for the measurement and inferring realistic response values of the complete instrument for the final application.

II. THEORY

A. Liquid crystals' response time

The response time of a nematic LCVR is the time required for the director vector of the LC molecules to be oriented from an initial to a final state induced by a driving electric field. The tilt of the molecules is the result of the equilibrium between the anchoring forces[7,9] between the LC molecules and the polyimide treatment deposited on the substrates, the elastic forces, and the applied electric field.[10–12] Therefore, the LC response time depends on several factors, including the LC layer thickness, viscosity, temperature, dielectric anisotropy, the surface treatment, the driving waveform frequency and amplitude, as well as the type and phase of the LC in use.[7,9,13–15]

The time range in which the nematic liquid crystals (NLCs) can operate is typically on the order of milliseconds. Another type of LC device which are nowadays used in the implementation of polarimeters are the ferroelectric liquid crystals (FLCs).[16–18] An important feature of FLCs is that these devices present faster response than NLCs (i.e., response times on the order of microseconds), and, therefore, they become the best option in applications where the acquisition velocity is a crucial factor. For the Solar Orbiter mission, the NLCs were the selected option since they have a suitable response time for the required image acquisition rate and also provide greater robustness compared to the FLCs[19] against the mechanical vibration environment during launch.

B. Modulation scheme and LCVR transitions

The PSAs based on LCVRs of the Solar Orbiter mission will carry out temporal polarization modulation by the application of a sequence of driving voltages that introduce different optical retardances. The PSA configuration, used in the PHI instrument, consists of two anti-parallel nematic LCVRs with their fast axes aligned at 45° with respect to each other, followed by a linear polarizer at 0° with respect to the fast axis of the first LCVR. The LCVRs will generate a modulation scheme of four different retardance states needed to solve the system of linear equations that will allow us to measure the four parameters of the Stokes vector of the incident light. The PSA will use the modulation scheme specified in Table I, where δ_{LCVR1} is the retardance of the first LCVR and δ_{LCVR2} is the retardance generated by the second LCVR. This modulation scheme corresponds to the Fe I line ($\lambda = 617.3$ nm) and was selected in order to obtain an invertible modulation matrix that will give maximum and homogeneous polarimetric efficiencies[20] to determine the four Stokes parameters of the incoming light.

TABLE I. Modulation scheme of PHI PSA.

Modulation	δ_{LCVR1} ($\lambda = 617.3$ nm) (deg)	δ_{LCVR2} ($\lambda = 617.3$ nm) (deg)
1	225	234.74
2	225	125.26
3	315	54.74
4	315	305.26

In order to meet the scientific requirements of the Solar Orbiter mission, each LC must be able to make an optical retardance change from the initial retardance state δ_o to the final state δ, governed by applied voltages V_1 and V_2, respectively, in less than 100 ms. Two different LCVRs compose the PSA. Nevertheless, both cells are very similar, and the response times studied and presented in this work will be for one of the two LCVRs. Then, the response times of six transitions will be studied for this LCVR, which are specified in Table II, and are in accordance with the PHI modulation scheme. $\Delta\delta$ corresponds to the total optical retardance change between the initial and the final retardance state.

C. Response time measurements

The standard method to measure the LC optical response time widely found in the literature[7,8] consists of a measurement of the output light from a system comprising a monochromatic light reaching crossed or parallel polarizers and the LC sample with its fast axis oriented to 45°. This method measures light intensity as a function of time, which is known as the optical response time. The optical response time is defined as the time period elapsed between 10% and 90% of the detected output signal. The equation governing the intensity response of this system is known and expressed as

$$I(t) = (I_{\max} - I_{\min})\sin^2\left(\frac{\delta_{LCVR}(V)}{2}\right) + I_{\min}, \quad (1)$$

where $\delta_{LCVR}(V)$ is the variable retardance as a function of the applied voltage of the LC cell and $I_{\max}$ and $I_{\min}$ are the

TABLE II. Retardance transition scheme, where $\delta_0(V_1)$ is the initial LCVR retardance state governed by the first voltage V_1 and $\delta(V_2)$, is the final LCVR retardance state governed by the final voltage V_2. $\Delta\delta$ is the total retardance change defined by $\Delta\delta = \delta(V_2) - \delta_0(V_1)$.

	$\lambda = 617.3$ nm				
Transition	$\delta_0(V_1)$ (deg)	V_1 (V)	$\delta(V_2)$ (deg)	V_2 (V)	$\Delta\delta$ (deg)
1	234.74	2.065	125.26	3.007	−109.48
2	125.26	3.007	54.74	5.757	−70.52
3	54.74	5.757	305.26	1.741	250.52
4	305.26	1.741	234.74	2.065	−70.52
5	225	2.119	315	1.703	90
6	315	1.703	225	2.119	−90

maximum and minimum intensities of the system, respectively. By normalizing[21] $I(t)$, we obtain

$$I_N(t) = \frac{I(t) - I_{\min}}{I_{\max} - I_{\min}} = \sin^2\left(\frac{\delta_{LCVR}(V)}{2}\right), \tag{2}$$

where $I_N(t)$ is the normalized intensity over time.

Nevertheless, the parameter required in polarimetric instruments, such as PHI and METIS, is the optical retardance temporal variation. This leads to different problems.

On one hand, the response time measured from the transmission intensity variations is not directly the optical retardance response time. Note that the light intensity is a square sinusoidal function of the optical retardance as shown in Eq. (2). The same response time should be obtained applying the same values of V_1 and V_2 and, therefore, δ_o and δ (see Table II) for LCVR. Nevertheless, different values of the optical response time will be measured starting from different points in the curve of Eq. (2) due to this dependence. It will be shown in Sec. IV.

On the other hand, the sensitivity of the system to the retardance change of the LC cell will have a noticeable dependence according to the area of the intensity curve. The sensitivity depends on the slope of function in Eq. (2) and is calculated by applying partial derivatives to this equation. Therefore, the sensitivity of the system to retardance changes is defined as

$$\frac{\partial I}{\partial \delta} = \cos\left(\frac{\delta}{2}\right) \cdot \sin\left(\frac{\delta}{2}\right). \tag{3}$$

Equation (3) and Fig. 1 show that the area with the highest sensitivity to retardance changes is the central zone of the output intensity curve where the retardance values of the sample are close to $n\pi/2$ (where $n = 1, 3, 5,\ldots$) radians. While the regions with the lowest sensitivity are near the null and maximum intensity where the sample retardance values are $n\pi$ radians. Additionally, we calculated the uncertainty in the retardance value as a function of the measurements of light intensity using the uncertainty propagation calculus of Eq. (2) (Fig. 2). The calculation is shown in Eq. (4) and plotted in Fig. 3,

$$\sigma_\delta = \sqrt{\frac{\sigma_I}{1 - I^2}}, \tag{4}$$

where σ_δ and σ_I are the uncertainty of the optical retardance and intensity, respectively.

It can be seen that the uncertainty is minimum in the central zone of the output intensity curve. Nevertheless, the uncertainty is maximized up to infinite values in areas close to the null and maximum intensity.

The area with the highest sensitivity to retardance changes and minimum uncertainty will be called the linear regime of the output intensity. On the contrary, the area with the lowest sensitivity and, therefore, the maximum uncertainty will be called the parabolic regime of the output intensity. Taking into account these calculations, the measurements of the response times must be performed in the linear regime since it minimizes the effect of the intensity dependence on the optical retardance and the measurement uncertainty propagation. Nevertheless, the starting point in the intensity light curve depends on the LCVR initial retardance of each specific transition. Therefore, we need to tune this starting point in order to measure the LCVR response times in the optimized conditions. The solution proposed in our experimental setup is the insertion of a Soleil-Babinet variable compensator, which is explained in Sec. II C 1.

1. Addition of a variable compensator

The insertion of a Soleil-Babinet variable compensator allows us to tune the optical retardance starting point of the response time measurements. Now, the equation governing the intensity response of this system is expressed as

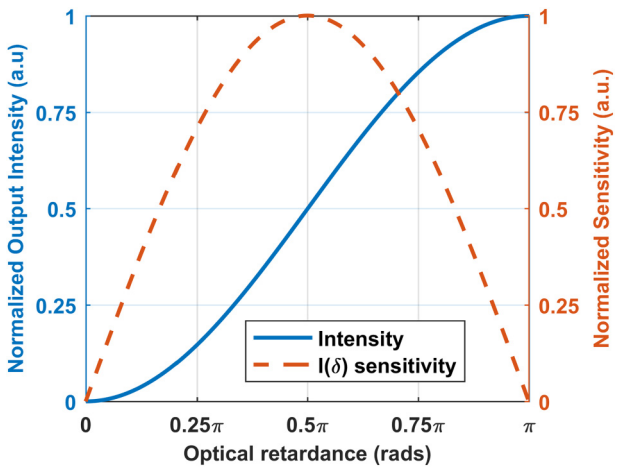

FIG. 1. Normalized intensity output of the system with crossed polarizers configuration and normalized sensitivity to retardance changes within a range from 0 to π radians.

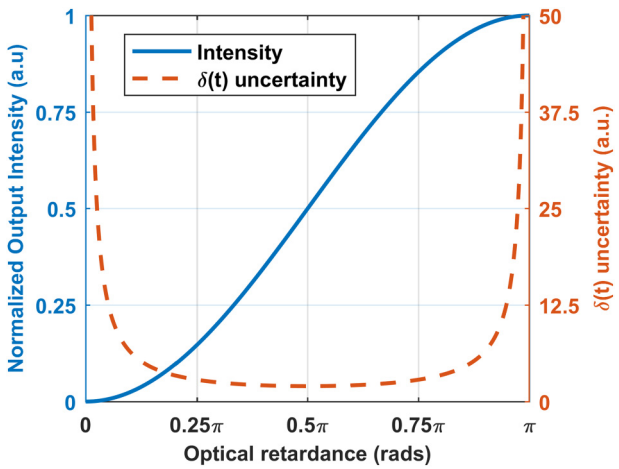

FIG. 2. Normalized intensity output of the system with crossed polarizers configuration and the uncertainty propagated in $\delta(t)$ inversion within a range from 0 to π radians.

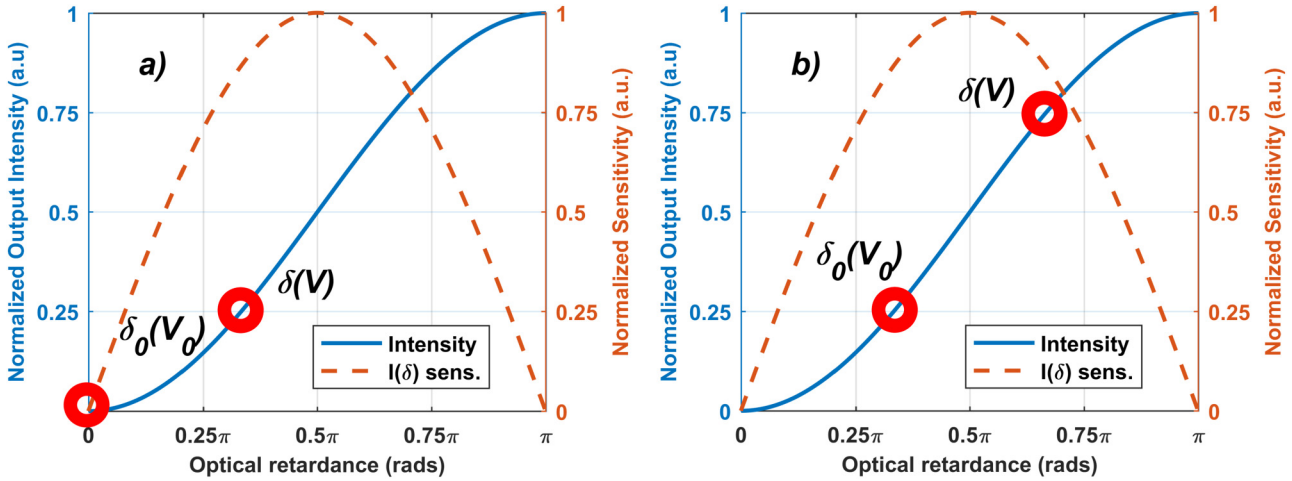

FIG. 3. Output intensity and $I(\delta)$ sensitivity for the same retardance shift transition studied in parabolic and linear regimes: (a) parabolic regime and (b) linear regime.

$$I_N(t) = \sin^2\left(\frac{\delta_T(V)}{2}\right), \tag{5}$$

where δ_T is the sum of the LCVR optical retardance (δ_{LCVR}) and the retardance of the compensator (δ_C). In the starting point of the transition, the Soleil-Babinet compensator retardance can be tuned. This allows us to locate the response signal of each LCVR specific transition in the desired regime of the output intensity and study the same transition under different conditions. As an example, the same transition studied in the parabolic regime and the linear regime is depicted in Figs. 3(a) and 3(b), respectively. The differences between the measurements in these two regimes are shown in Sec. IV.

2. Wavelength selection

Another problem in the determination of the response times is when the transitions studied overcome 180° of the retardance change. For example, this is the case of the third transition of the PHI modulation scheme (Table II) that shows a retardance change of 250.52° at $\lambda = 617.3$ nm. This produces a maximum in the output detected intensity signal followed by a decrease as shown in Fig. 4(a). The analysis of the response time in this transition is complicated and less accurate. Additionally, we cannot study this transition in the linear regime or in the parabolic regime separately. Taking into account the Cauchy dispersion of the LC mixture birefringence, a longer wavelength of $\lambda = 987.7$ nm was selected for the experimental setup in order to have a monotonically increasing output signal as shown in Fig. 4(b). Note that, applying the same driving voltages, the dynamic behavior of the device is maintained.

D. Inversion to retardance δ and molecular mean tilt θ

We can calculate the optical retardance temporal variation using the experimental values of the obtained light intensity as a function of time and from inversion

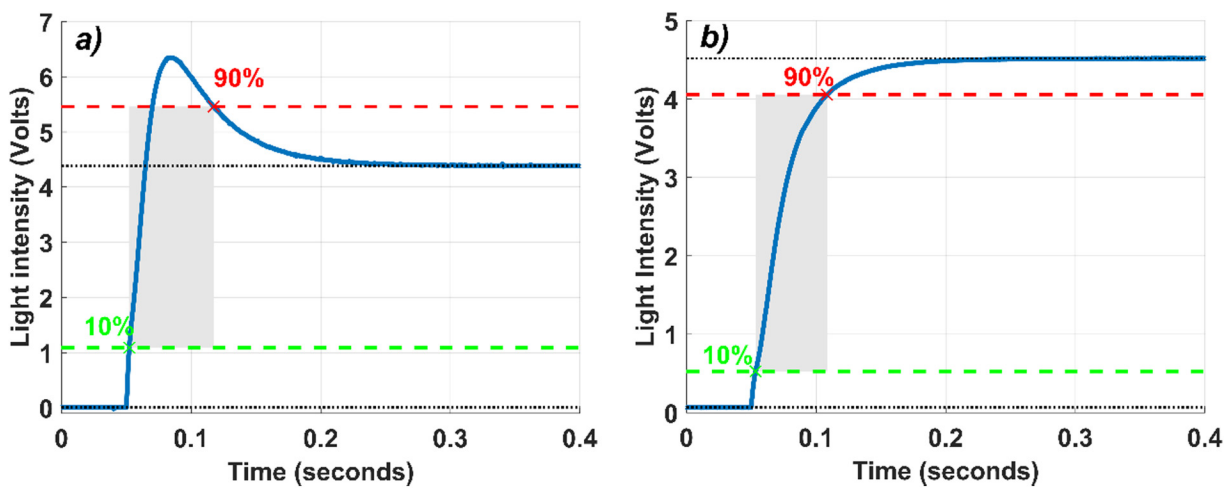

FIG. 4. (a) Output intensity of transition 3 of the PHI retardance scheme using $\lambda = 617.3$ nm. (b) Output intensity of transition 3 of the PHI retardance scheme using $\lambda = 987.7$ nm.

of Eq. (2),

$$\delta_{LCVR}(t) = 2\,\mathrm{asin}\left(\sqrt{I_N(t)}\right). \tag{6}$$

The study of $\delta(t)$ will allow analyzing how the LCVR retardance variations over time influence the modulation efficiencies of polarimetric instruments. From $\delta(t)$, we also calculate the temporal variation of the LC molecules mean tilt using the well-known following equations:[22]

$$\delta_{LCVR}(t) = \frac{2\pi d}{\lambda}(n_{eff}(t) - n_o), \tag{7}$$

$$n_{eff} = \frac{n_e n_o}{\sqrt{n_e^2 \sin^2(\theta) + n_o^2 \cos^2(\theta)}}, \tag{8}$$

where d is the thickness of the LCVR cell, λ is the wavelength, n_e and n_o are the extraordinary and ordinary LC refractive indices, n_{eff} is the extraordinary LC effective refractive index, and θ is the molecular mean tilt. Using Eqs. (5) and (6), we calculate the LC mean tilt as

$$\theta(t) = \mathrm{asin}\left(\sqrt{\frac{n_o^2 n_e^2}{n_{eff}^2(t)\,(n_e^2 - n_o^2)} - \frac{n_o^2}{(n_e^2 - n_o^2)}}\right). \tag{9}$$

The temporal variation of the LC molecules mean tilt will provide the experimental data needed to fit Ericksen–Leslie partial derivatives equation solutions that describe the liquid crystal molecular dynamics.[10–12] Thus, we will be able to determine the physical constants such as Frank elastic constants and Leslie–Ericksen viscosity coefficients and, therefore, study the LC dynamic properties. Additionally, in the context of a space instrument, it will allow evaluating these LC properties under the environmental space conditions such as ultraviolet and gamma irradiation or vacuum and temperature tests.

III. EXPERIMENTAL DETAILS

A. Experimental setup

A scheme of the experimental setup is shown in Fig. 5. The light source used is a Thorlabs L980P030 laser diode with the wavelength stabilized at $\lambda = 987.7$ nm. The linear polarizers, arranged in crossed configuration, are Thorlabs LPVIS100-MP2 with a high extinction ratio in the selected wavelength of $\lambda = 987.7$ nm. The variable compensator is a Thorlabs SBC-IR Soleil-Babinet type, remotely controlled from a Newport SMC100CC single axis motion controller. The LCVR under test is an LC cell composed of Merck ZLI-3700-000 nematic mixture with antiparallel alignment and a thickness of 10 μm. This LCVR cell belongs to the same manufacturing batch of the LCVR used in PHI and METIS instruments. In the setup, the fast axis of the LCVR under test and the variable compensator are parallel to each other and oriented to 45° with respect to the polarizers.

A set of aspheric lenses are used to collimate the light beam in order to assure normal incidence to the LCVRs. After the second polarizer, the beam is focused by a convergent lens on the photoreceiver. The high speed New Focus 1621 photodetector that assures a response speed of 50 ns is used. The LCVR voltage driving is carried out with a Tektronix AFG3011C function generator, modulating the amplitude of a 2 kHz square carrier signal between the initial and the final voltage of each retardance transition. The LCVR cell is thermal stabilized at 40.0 ± 0.1 °C.

B. Measurements

The six LCVR transitions of the PHI instrument have been measured in the parabolic and linear regimes using the setup described in Sec. III A. The parabolic regime is achieved by starting from an intensity null, where the variable compensator retardance is $\delta_C = 2n\pi - \delta_0(V_1)$. The linear regime is achieved by locating the transition output intensity signal centered in the linear regime, where the variable compensator retardance is $\delta_C = 0.5[(2n+1)\pi - \Delta\delta] - \delta_0(V_1)$. In both cases, n is an integer whose value is $n = 0, 1, 2, \ldots$.

In addition, we invert the light intensity measurement to calculate the optical retardance and the LC molecular mean tilt response times using Eqs. (6) and (9). To calculate the LC molecular mean tilt, we use $n_e = 1.563 \pm 0.002$ and $n_o = 1.473 \pm 0.002$ of the LC mixture ZLI-3700-000 at a

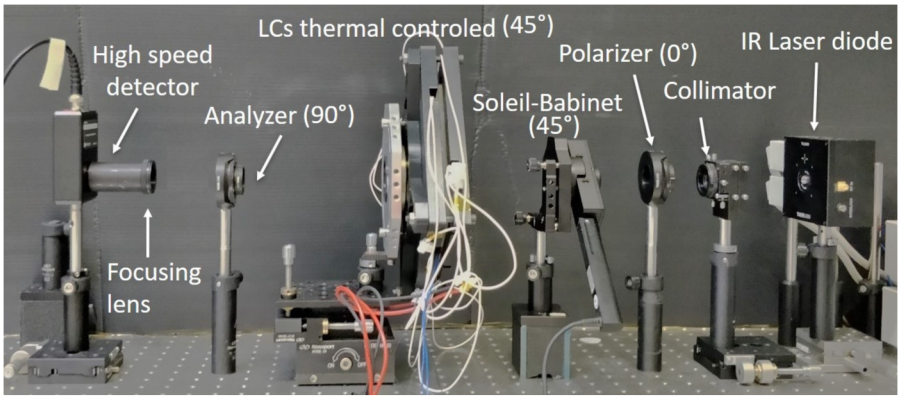

FIG. 5. Experimental setup.

TABLE III. Response times (RT) and standard deviation (STD) of the six PHI retardance transitions performed in the LCVR at 40 °C in the parabolic regime.

	Intensity		Retardance		Tilt	
Transition	RT (ms)	STD (ms)	RT (ms)	STD (ms)	RT (ms)	STD (ms)
1	20.42	0.06	18.7	0.09	19.45	0.07
2	4.02	0.03	3.56	0.04	3.79	0.04
3	54.9	0.1	59.4	0.2	52.7	0.3
4	57.2	0.2	53.0	0.1	53.6	0.1
5	86.5	0.2	78.1	0.2	76.9	0.2
6	53.63	0.06	49.58	0.08	50.36	0.09

TABLE IV. Response times (RT) and standard deviation (STD) of the six PHI retardance transitions performed in the LCVR at 40 °C in the linear regime.

	Intensity		Retardance		Tilt	
Transition	RT (ms)	STD (ms)	RT (ms)	STD (ms)	RT (ms)	STD (ms)
1	17.27	0.04	18.13	0.02	19.05	0.05
2	3.163	0.008	3.206	0.007	3.50	0.02
3	49.2	0.2	55.3	0.2	48.4	0.3
4	50.1	0.08	50.82	0.05	51.73	0.07
5	71.8	0.1	73.2	0.1	71.36	0.1
6	47.53	0.01	48.51	0.03	49.66	0.02

wavelength of $\lambda = 987.7$ nm obtained using the Cauchy[23,24] dispersion and LCVR thickness, which is $10\,\mu$m.

IV. RESULTS AND DISCUSSION

A. Comparison between parabolic and linear regimes

The results obtained in the response time measurements of the LCVR cell and subsequent inversions to the optical retardance and the LC mean tilt for the parabolic and linear regimes are shown in Tables III and IV, respectively. The results shown are the mean and standard deviation calculated from 20 consecutive measurements for each transition.

In the case of the measurements in the parabolic regime (Table III), it can be observed that the response times directly obtained from the intensity experimental data, i.e., the optical response time, are slower than the inverted retardance and molecular mean tilt data. The only exception is the case of transition 3. For this case, the nonlinear intensity dependence on the optical retardance has provided a lower value. In particular, this specific transition has the highest change in the optical retardance. In addition, the retardance response time and the mean tilt response times are very similar to each other for each transition.

In the case of the measurements in the linear regime shown in Table IV, the results directly obtained from the experimental intensity data, i.e., the optical response time, show values very similar to those obtained after the inversion to retardance and tilt. Again, the only exception is transition 3, where the response time obtained from the intensity measurements yields faster and higher differences than those calculated after inversion to retardance and tilt. This behavior is due to the same reason explained previously, Sec. IV B will show a discussion explaining these experimental results.

The comparison between results in Tables III and IV is shown in Fig. 6. It can be observed that the optical response times when the transition starts from an intensity null in the parabolic regime are slower than the results in the linear regime of the same transition. Additionally, the rest of the values, optical retardance, and mean tilt are more similar to those values of the optical response time in the linear regime. This is due to the intensity transmission dependence on the LCVR optical retardance as described in Eq. (2) and

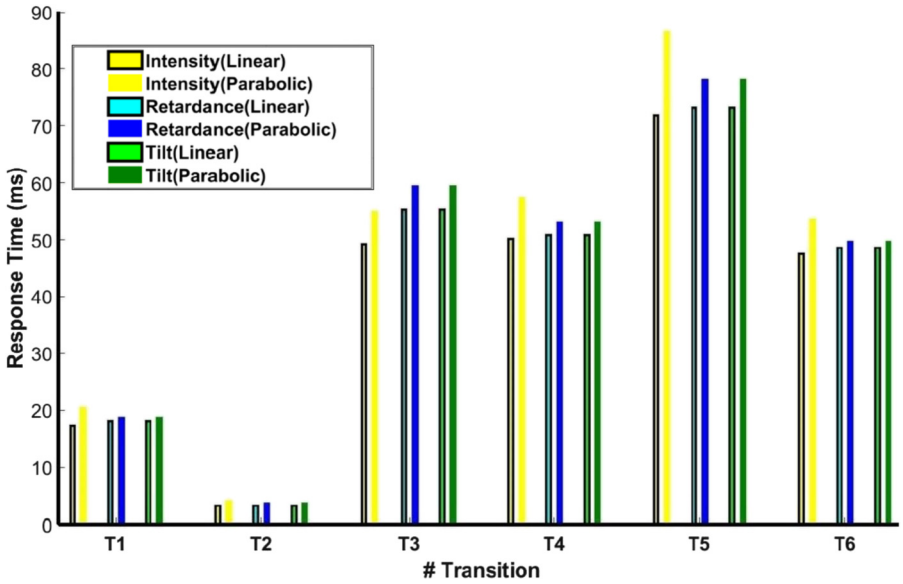

FIG. 6. Bar plot comparing response time measurements of the LCVR in parabolic and linear regimes.

TABLE V. Response times of the simulations of transition 3. $\delta_{LCVR}(t)$ column shows the response time of retardance over time, $I(t)$ parab. (null) are the values calculated from $I(t)$ with transition intensity starting from a null, $I(t)$ linear are the values calculated from $I(t)$ centering the transition on linear regime, and $I(t)$ parab. (max.) are the values calculated from $I(t)$ with transition intensity ending at a maximum.

	Response time (ms)			
	$\delta_{LCVR}(t)$	$I(t)$ parab. (null)	$I(t)$ linear	$I(t)$ parab. (max.)
Case $\Delta\delta$	59.519	54.905	49.230	33.235
Case $\Delta\delta/2$	59.519	70.813	58.223	28.223

explained in Sec. II B. This contribution in the optical retardance response is higher in the parabolic regime than in the linear regime. This means that the optical response measurements carried out in the parabolic regime near an intensity null are overestimated.

Based on these conclusions and the calculation of the sensitivity and uncertainty propagation of Sec. II B, the optimized conditions to measure response times are in the linear regime. These conditions for all the LCVR transitions can only be achieved using a variable compensator and the suitable wavelength as in the experimental setup proposed in our work, which allows tuning the starting point in the light intensity measurements.

B. Transition 3 results and discussion

The system response for transition 3 has been numerically simulated using Eq. (5). δ_C is an offset that allows the transition to be placed in the appropriate regime, simulating the Soleil-Babinet compensator. δ_{LCVR} are the optical retardance values resulting from inverting experimental values of $I(t)$ to $\delta(t)$, with $I(t)$ being the intensity values of transition 3 in the linear regime at $\lambda = 987.7$ nm. The transition has been simulated for three different cases: starting with null intensity, centered in the linear regime, and ending with the maximum intensity. The response times of these three cases along with $\delta_{LCVR}(t)$ have been calculated and are shown in the first row of Table V.

Later, we have simulated the use of a longer wavelength that leads to retardance values for which the difference in retardance $\Delta\delta$ is half the one obtained with $\lambda = 987.7$ nm. Then, the same simulations and response time calculations as in the previous case have been performed. These results are shown in the second row of Table V.

It can be seen that the results of the simulation for $\Delta\delta$ match perfectly with the experimental results shown in Tables III and IV. Additionally, the results for $\Delta\delta/2$ show the same trend as the rest of transitions presented in this study, where the response time of the $I(t)$ data starting from the parabolic regime is slower than those measured in the linear regime and, in turn, this last value is close to the one calculated on the $\delta(t)$ data.

From this simulation, we can conclude that the effect of the transmitted intensity nonlinear dependence on the optical retardance overestimates the response time by starting the transition in the parabolic regime and underestimates it when the transition ends in the parabolic regime. Hence, the different behavior found in transition 3 is due to the fact that its retardance difference $\Delta\delta$ for $\lambda = 987.7$ nm is wider than the other transitions. Therefore, it cannot be only measured in the linear regime, and the two effects contribute to the total measured response time. This behavior can be avoided by reducing the optical path with the use of a longer wavelength and measuring in the linear regime.

C. Exponential fitting of the LCVR transitions

Once the LCVR transitions have been measured in the optimized conditions that allow the accurate determination of the optical retardance and the mean tilt temporal variation, the LC dynamics can be studied. This will provide information to parameterize solutions of the differential equation of Ericksen–Leslie and obtain the physical parameters of the liquid crystal molecules. As an example, a decay transition of the LCVR studied in the linear regime has been exponential fitted (Fig. 7). Under certain conditions, the retardance change of a liquid crystal cell can be approximated to an exponential equation[9,25] as follows:

$$\delta(t) = \Delta\delta \cdot \exp\left(-\frac{2t}{\tau}\right), \tag{10}$$

where $\delta(t)$ is the optical retardance as a function of time, $\Delta\delta$ is the total retardance change of the transition, t is the time,

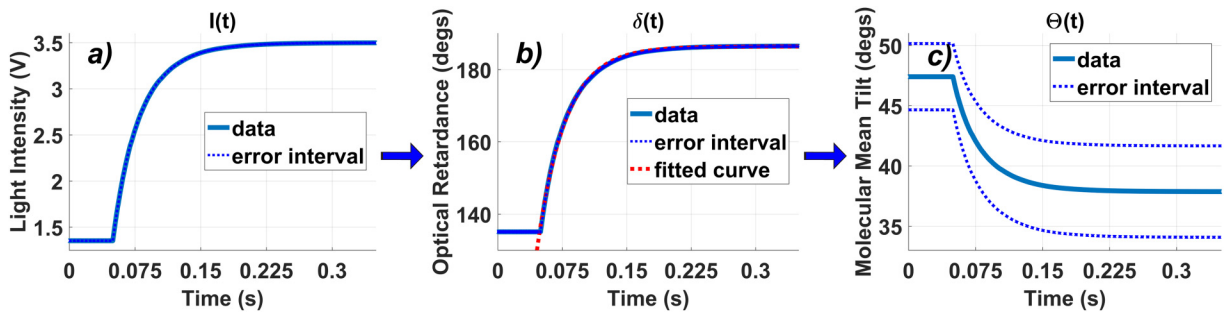

FIG. 7. Response time measurements in the linear regime of LCVR transition 5 at 40 °C fitted to exponential equation. (a) Light intensity measurements. (b) Optical retardance response times by inversion using Eq. (6). (c) Molecular mean tilt response times by inversion using Eq. (9). The three plots show an error interval calculated by uncertainty propagation.

and τ is the LC director reorientation time. The latter is related to the physical parameters of the LC dynamics that will be studied in future works under the different environmental conditions of a space mission.

V. CONCLUSIONS

In this work, we present an experimental setup that improves the standard method to measure LCVR response times. Thanks to the proper selection of the wavelength and the use of a Soleil-Babinet variable compensator in this experimental setup, we increase the accuracy of the measurements. The use of a variable compensator allows for tuning the starting point in the light intensity measurements. This allows selecting the optimized conditions that increase the accuracy of the measurements and reducing the effect of the transmitted intensity nonlinear dependence on the optical retardance.

The measurements of the six transitions in the PHI modulation scheme of an LCVR cell show that there is a noticeable difference between the measurements made in parabolic and linear regimes. The comparison of the values obtained for both regimes with those obtained via inversion to $\delta(t)$ and $\theta(t)$ indicates that the measurements performed in intensity in the parabolic regime are overestimated or underestimated. In addition, based on the calculation of partial derivatives and uncertainty propagation, the highest sensitivity and minimum uncertainty area to measure optical retardance values is the linear regime. Based on these results, the optimized conditions to measure response times is in the linear regime, which only can be achieved for all LCVR transitions using a variable compensator as in our experimental setup proposed in our work. In the case of the setup that does not allow the use of a variable compensator, we recommend inverting to $\delta(t)$ or $\theta(t)$ to obtain a more accurate response time measurement.

Finally, an accurate determination of the variation of the LCVR optical retardance as a function of time allows us to calculate accurately the temporal variation of the liquid crystal molecules mean tilt. In future works, this will provide the physical parameters of the LC dynamics and how they are affected in the environmental conditions of a space instrument.

ACKNOWLEDGMENTS

The authors are very grateful to all the members of the SO/PHI team and the INTA team, in particular. This work would not have been possible without them. This project was funded by the Ministerio de Ciencia, Innovación y Universidades (No. ESP2016-77548-C5-4-R).

[1]A. Álvarez-Herrero *et al.*, Proc. SPIE **9613**, 96130I (2015).
[2]S. K. Solanki *et al.*, "The polarimetric and helioseismic imager on solar orbiter," Astron. Astrophys. (to be published).
[3]E. Antonucci *et al.*, "Metis: the Solar Orbiter visible light and ultraviolet coronal imager," Astron. Astrophys. (to be published).
[4]V. Martínez Pillet *et al.*, Sol. Phys. **268**, 57 (2011).
[5]A. R. Tiwary, S. K. Mathew, A. R. Bayanna, P. Venkatakrishnan, and R. Yadav, Sol. Phys. **292**, 49 (2017).
[6]T. Horn and A. Hofmann, Astr. Soc. P. **184**, 33 (1999).
[7]D.-K. Yang and S.-T. Wu, *Fundamentals of Liquid Crystal Devices* (Wiley, New York, 2015).
[8]Y. Utsumi, T. Kamei, R. Naito, and K. Saito, Mol. Cryst. Liq. Cryst. **434**, 9/[337] (2005).
[9]H. Wang, *Studies of Liquid Crystal Response Time* (University of Central Florida, Orlando, FL, 2006).
[10]I. W. Stewart, *The Static and Dynamic Continuum Theory of Liquid Crystals: A Mathematical Introduction* (Taylor & Francis, London, 2004).
[11]P. G. de Gennes and J. Prost, *The Physics of Liquid Crystals* (Clarendon, Oxford, 1998).
[12]S. Chandrasekhar, *Liquid Crystals* (Cambridge University, Cambridge, 1992).
[13]A. F. Naumov and G. D. Love, Proc. SPIE **4124**, 57 (2000).
[14]S. Zhang, C. Chen, H. Jiang, H. Gu, X. Chen, C. Zhang, and S. Liu, J. Opt. **21**, 065605 (2019).
[15]K.-C. Lang and H.-K. Teng, Appl. Opt. **56**, 7718 (2017).
[16]C. Xu, Z. Qu, X. Zhang, C. Jin, and X. Yan, Appl. Opt. **45**, 8428 (2006).
[17]J.-M. Malherbe, T. Roudier, P. Mein, J. Moity, and R. Muller, Astron. Astrophys. **427**, 745 (2004).
[18]A. Peinado, A. Lizana, and J. Campos, Proc. SPIE **8873**, 88730S (2013).
[19]V. Lapanik, V. Bezborodov, G. Sasnouski, and W. Haase, Liq. Cryst. **40**, 1391 (2013).
[20]J. C. del Toro Iniesta and M. Collados, Appl. Opt. **39**, 1637 (2000).
[21]J. C. Gladish and D. D. Duncan, Proc. SPIE **7566**, 756609 (2010).
[22]L. Vicari, *Optical Applications of Liquid Crystals* (CRC, Philadelphia, PA, 2003).
[23]P. García Parejo and A. Álvarez-Herrero, Opt. Mater. Express **9**, 2681 (2019).
[24]J. Li, C.-H. Wen, S. Gauza, R. Lu, and S.-T. Wu, J. Disp. Technol. **1**, 51 (2005).
[25]H. Wang, T. X. Wu, X. Zhu, and S.-T. Wu, J. Appl. Phys. **95**, 5502 (2004).